Journal of the Korean Society of Propulsion Engineers
Vol. 18, No. 5, pp. 43-53, 2014

Research Paper
DOI: http://dx.doi.org/10.6108/KSPE.2014.18.5.043

충격파 터널을 이용한 고속추진기관 시험 연구

박기수[a] · 변종렬[b,*] · 최호진[b] · 진유인[c] · 박 철[a] · 황기영[b]

High Speed Propulsion System Test Research Using a Shock Tunnel

Gisu Park[a] · Jongryul Byun[b,*] · Hojin Choi[b] · Yuin Jin[c] · Chul Park[a] · Kiyoung Hwang[b]
[a]*School of Mechanical, Aerospace and Systems Engineering, Korea Advanced Institute of Science and Technology, Korea*
[b]*Advanced Propulsion Technology Center, Agency for Defense Development, Korea*
[c]*Accurately Guided Vehicle System, University of Science and Technology, Korea*
[*]*Corresponding author. E-mail: joy2bjr@gmail.com*

ABSTRACT

Shock tunnels are known to be capable of simulating flow-field environments of supersonic and hypersonic flights. They have been operated successfully world-wide for almost half a century. As a consequence of the strong interest in hypersonic vehicles in Korea, attention has been given on this type of facility and so an intermediate-sized shock tunnel has lately been built at KAIST. In the light of this, this paper presents our tunnel performance and some of the model scramjet test data. The freestream flow used in this work replicates a supersonic combustor environment for a Mach 5.7 flight speed.

초 록

충격파 터널은 초음속 및 극초음속 비행조건의 유동장을 지상에서 가장 유사하게 모사할 수 있는 시험설비로서, 거의 반세기 동안 전 세계적으로 유용하게 운용되고 있다. 국내의 극초음속 비행체에 대한 많은 관심의 결과로 충격파 시험장치에 대해 주목하고 있으며, 최근에 KAIST에서는 중간 크기의 충격파 터널을 갖추게 되었다. 본 논문은 개발된 충격파 터널의 성능과 최근 수행된 모델 스크램제트 시험자료를 제시하고 있다. 본 연구에서 모사된 자유흐름 유동조건은 마하수 5.7 비행속도에 해당하며, 이러한 비행조건에서 스크램제트의 초음속 연소기내에 유동 환경을 모사하였다.

Key Words: Shock Tube(충격파관), Shock Tunnel(충격파 터널), Scramjet(스크램제트), Hypersonic (극초음속), Supersonic Combustor(초음속 연소기)

1. Introduction

Received 25 November 2013 / Revised 22 August 2014 / Accepted 1 September 2014

pISSN 1226-6027 / eISSN 2288-4548

Scramjet is an air-breathing supersonic combustion ramjet engine that can propel a vehicle to hypersonic speeds[1]. To develop successful scramjet, an extensive amount of

experiments need to be conducted to improve its performance. For this purpose, utilization of wind tunnel facilities, which can produce flight values of temperature and velocity, is required.

The standard blow-down wind tunnels can produce hypersonic flows. Considering test section power levels per unit area which increase as the cube of the airstream velocity[2], it is clear that the associated power levels when operating such flow conditions using the blow-down tunnels are large. Also, high temperatures involved in supplying air at such velocities make the operation of the tunnels difficult. Because of this, it is unlikely that the blow-down tunnel technology can be applied in scramjet testing.

An alternative way of producing high wind tunnel power levels is to rapidly add energy to the test gas immediately before it is allowed to expand to produce inflows in the test section. This technique is known as an impulse type. Using this technique, the incoming flows within a steady state in the test section usually last for only a few milliseconds, but contain high power levels. Also, high temperatures are sustained. The impulse facility that has been used for this purpose is known as a shock tunnel. Because the shock tunnel can produce freestream flows that replicate a supersonic combustor environment associated with an air-breathing engine flying at hypersonic speeds, it is regarded as the viable means for the scramjet testing.

To operate the scramjet efficiently in the Mach numbers of 6 and above(a long flight range), hydrogen fuels generally have been considered. But compared with hydrogen, hydrocarbon fuels have several advantages such as higher densities(reducing dry mass, aerodynamic drag, and increasing payload ratio), lower cost, and ambient storability at reduced operational costs. There is a general consensus that hydrocarbon fuels can be used when flight speed is up to Mach 6[3].

The shock tunnels have been used by many investigators in various countries to test a high Mach number hydrogen-fueled scramjet system[1,2,4-9]. Regarding the hydrocarbon fuels, however, a reliable set of experimental data is sparse[10,11].

Korea Aerospace Research Institute(KARI) has successfully conducted Mach 5 scramjet testing using a blow-down type engine test facility[12]. Although this facility can well produce relatively low total temperature (~1100 K) and so an intermediate Mach number flow, it is incapable of matching all flow properties above a flight Mach number well above 5. To date, there is no hypersonic facility available in this country that can produce flight conditions varying from intermediate to high Mach number flows.

Therefore, the KAIST research team has lately built an intermediate-sized shock tunnel. A series of experiments using the hydrocarbon fuel, ethylene, is now actively in progress. The aims of this work are to verify that the shock tunnel is capable of conducting scramjet combustion test and also to inform nationally the overall design, manufacture, and performance testing skills of high speed propulsion system using the shock tunnel. This paper covers three aspects: (1) the method of characterizing the tunnel flow condition, (2) our tunnel performance and, (3) some of the recent scramjet test data.

2. Shock Tunnel

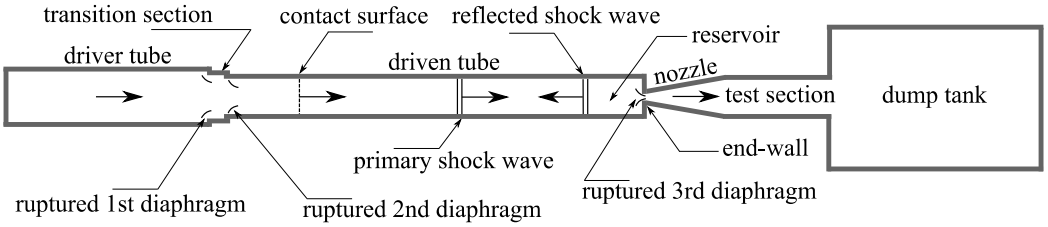

Fig. 1 Schematic of the KAIST shock tunnel.

Fig. 1 and 2 show schematic and photographs of the KAIST shock tunnel, respectively. The tunnel is about 13 m long. It consists of a shock tube, a nozzle, a test section, and a dump tank. The shock tube contains three axisymmetric chambers: a driver tube, a transition section, and a driven tube. They are initially separated by the first and the second diaphragms. The diaphragms are made of a 2.5 mm thick polycarbonate sheet. The gas used in the driver tube and the transition section is pure cold helium.

Before firing, the diaphragms are held in position. The gas in the driver tube and the transition section are then pressurized. When the desired value of pressure is reached, a valve mounted in the wall of the transition section is opened to let the gas in this section to escape into the atmosphere. This would then increase the pressure difference across the first diaphragm. When the pressure difference across the diaphragm exceeds the limit that the diaphragm can bear, the diaphragm ruptures and the high pressure gas in the driver tube fills the transition section. The second diaphragm then cannot bear the pressure difference across it and so it ruptures. This causes the gas in the driver to flow downstream into the driven tube.

The driver tube gas is now pushing the driven tube gas. An interface between the driver and the driven gases is called a contact surface. The principle of gas dynamics dictates that a sudden discontinuity in pressure occurs in the driven tube gas. This discontinuity is called a shock wave.

Fig. 2 Photographs of the KAIST shock tunnel.

The third diaphragm is made of a 0.11 mm thick polyethylene sheet, which initially separates the test gas(driven tube gas) from the test section gas. When the shock wave reaches the end-wall of the driven tube, the third diaphragm ruptures and the shock wave reflects. It then moves backward against the flow. This shock wave is called a reflected shock wave and the region behind it is called a reservoir(where velocity is nearly stagnant).

The compressed test gas is then processed by steady expansion which expands into a nozzle and reaches an experimental model that is mounted in the test section. A dump tank

is used as gas storage so that a large amount of gas can be vented after the experiment.

3. Computational Details

One flow condition was used in this work. Thermodynamic properties of the freestream flow were calculated by dividing parts into two stages(shock tube and nozzle). After the nozzle calculation, the obtained freestream properties were further validated using scramjet simulation results without fuel injection and cavity. The details for the three stages are given next.

3.1 Shock Tube

This stage covers the region from the beginning of the driver tube to the end-wall of the driven tube. Table 1 summarizes the shock tube pressure filling condition. In the table, L, D, and He denote length, internal diameter, and helium, respectively.

Thermodynamic properties were calculated using a time-dependant one-dimensional code L1d2. This is an in-house code from The University of Queensland in Australia[13]. The code formulates the gas dynamics through Lagrangian discretization of gas slugs.

The regions of gas slugs were divided into a set of control masses that were tracked throughout time in one spatial coordinate. Viscous effects were included and the gas was assumed to be thermally perfect. Details regarding the governing equations used in the code can be found in Refs.[13,14].

Table 1. Shock tube pressure filling condition.

Component	Gas Type	Filling Pressure (MPa)
Driver tube L=2.1 m, D=0.19 m	He	4
Transition section L=0.24 m, D=0.15 m	He	2
Driven tube L=7.0 m, D=0.13 m	Air	0.05

3.2 Nozzle

The nozzle consists of a converging, a throat, and a diverging sections. They were all two dimensional. The converging and the diverging sections were of a wedged-type. The length of the throat and the diverging sections were 30 mm and 600 mm, respectively. The height of the throat and the diverging sections were 15 mm and 150 mm, respectively. The wedged-type nozzle can produce slightly diverging and expanding flow at the nozzle exit compared with that of a contoured-type. Referring to various existing shock tunnel studies, however, it is known that this level of non-uniformity is found to be not serious[15-17].

Flow properties were calculated using a compressible Navier-Stokes solver Eilmer3 which is also an in-house code from The University of Queensland[18]. The code performs time integration of Navier-Stokes equations using cell-centered finite-volume formulation. The solver uses a multiple-block structured mesh. The mass, momentum, energy, and species flux between finite volume cells were calculated using an ADAPTIVE scheme. 791 x 63 (49,833) grid cells were used.

In the simulation, the surface was assumed to be non-ablative, non-catalytic, and its temperature was set at 293 K. A Park's two temperature model[19] was incorporated in the code. This model considers thermal energy into two modes: (1) translational and rotational energy in the 'translational-rotational' mode denoted as temperature T_{tr} and, (2) vibrational

and electronic energy in the 'vibro-electronic' mode denoted as temperature T_{ve}. Flow was regarded laminar throughout.

3.3 Scramjet

3.3.1 Model assembly

Fig. 3 shows a cross-sectional view of the scramjet model assembly. The scramjet was mounted in the test section that is connected to the nozzle block. The leading edge of the scramjet was located at about the nozzle-exit.

The scramjet consists of a contoured-wedge, a main flat body, a cowl, and a fuel injection module. The total length of the model was 390 mm. The height of the main body was 68 mm. The distance from the upper wall of the main body to the lower wall of the cowl (combustor height) was 20 mm. The width of the main body was 59.5 mm. The thickness of the cowl was 4 mm and its front area was chamfered.

Between the cowl and the main body, a pair of BK7 optical windows were side-mounted so that flow-fields can be visualized using a high speed camera. Along the upper wall of the main body, surface pressures were measured using 111A21 series PCB piezoelectric transducers. They were capable of measuring the pressures in the range of 0 to 689 kPa. The sensitivity of the sensors were typically 7.2~7.4 mV/kPa. The transducers were all flush mounted. The surface pressures were measured at four different locations. They were located at 0.22 m, 0.26 m, 0.29 m, and 0.32 m from the scramjet leading edge. Other locations shown in Fig. 3 were flush mounted using vacuum fillers.

Inside the main body, the fuel injection module was mounted. The injection mechanism

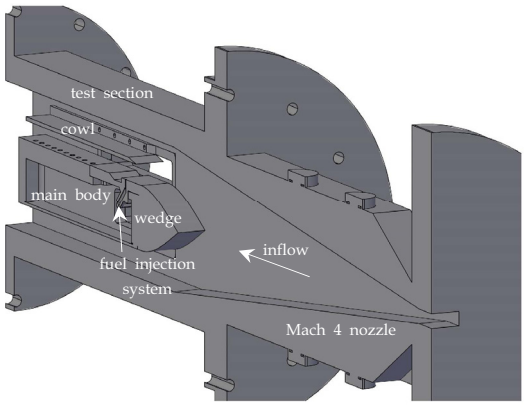

Fig. 3 A cross-sectional view of the scramjet model mounted in the test section.

was operated using a dual-mode high speed solenoid valves(General Valve Series 9, Iota One Controller) which allow near-constant injection flow rates during a steady flow test time period[10]. The fuel was supplied from a high pressure chamber that was individually connected to the solenoid valves through two flexible tubes. The tubes were joined using a T-pipe and then engaged to a CSLA-4-4U positional male elbow which was connected to a 1.2 mm diameter fuel injection orifice.

Various models with and without a cavity were used in the experiment. For each test, one model was mounted at one time. Details for each of the model and their associated experimental data are presented in Ref.[20].

3.3.2 Flow-field without fuel injection and cavity

The steady laminar flow simulation without the fuel injection and cavity was performed using the Eilmer3 code. The purpose for this simulation was to validate the freestream flow condition and also to obtain base-line data to compare with the experiment.

Fig. 4 shows a computational domain of the scramjet model. In total, 50,490 grid cells were used.

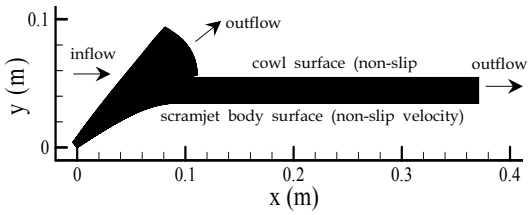

Fig. 4 A computational domain of the scramjet model.

In the figure, x and y denote distance along the horizontal and the vertical planes from the scramjet leading edge, respectively. The external boundary for the inflow on the left-hand side of the mesh was approximately aligned to the oblique shock wave angle to capture the gradients of shock as best as possible to improve solution convergence. The external boundary for the outflow is on the right-hand side of the mesh as well as the curved-edge above the cowl. The multiple block grid consisted of 40 blocks that were interconnected node to node. To resolve the boundary layer, the mesh was highly refined towards the main body and the cowl surfaces. Along the surfaces, a non-slip velocity condition was employed.

In the calculation, the structured mesh was used in the entire domain of the flow-field. The steady state flow properties obtained from the transient nozzle flow simulation were used as the inflow condition. The surface temperature was set at 293 K. The two temperature model was incorporated.

4. Results and Discussion

4.1 Shock Tube

Fig. 5 compares measured(Exp.) and calculated(CFD) wall static pressures along the driven tube. The wall pressures were measured using PCB transducers that were all flush mounted. At the end-wall, one PCB transducer was again flush mounted. Various shots of pressure signal traces are included to show the shot-to-shot repeatability.

In the figure, the times (t) are synchronized with respect to flow arrival time at station (1). Stations (1) and (2) are located at 0.1 m and 6.1 m from the beginning of the driven tube. Station (3) represents the end-wall. Because there is a slight time offset of the diaphragm rupture between the measurement and the calculation, to make direct comparison, the times for the calculated results are synchronized with respect to the measurement at the station (1).

The agreement between the experiment and the calculation is quite good except for the pressure trace measured at the station (1). This is thought to be due to the consequence of the L1d2 code which tends to initially overestimate the shock speed and so the pressure in the region vicinity of the 2nd diaphragm rupture.

At the end-wall, the measured pressure during a steady flow is 4.49(±3.8%) MPa. The calculated pressure is 4.69(±9.9%) MPa, which differs by 4.5% from the experiment. The flow seems to be steady up to about 1.0 msec with respect to the shock wave arrival. The shock wave speed was measured based on the shock arrival at the stations (2) and (3). The measured shock speed is 1180 m/sec. The calculated shock speed is 1200 m/sec, which differs by 1.7% from the experiment.

4.2 Nozzle

Fig. 6 compares the measured pitot pressure with that of the calculated values at the nozzle-exit center. In the figure, the time is synchronized with respect to the shock arrival at the end-wall. Various shots of signal

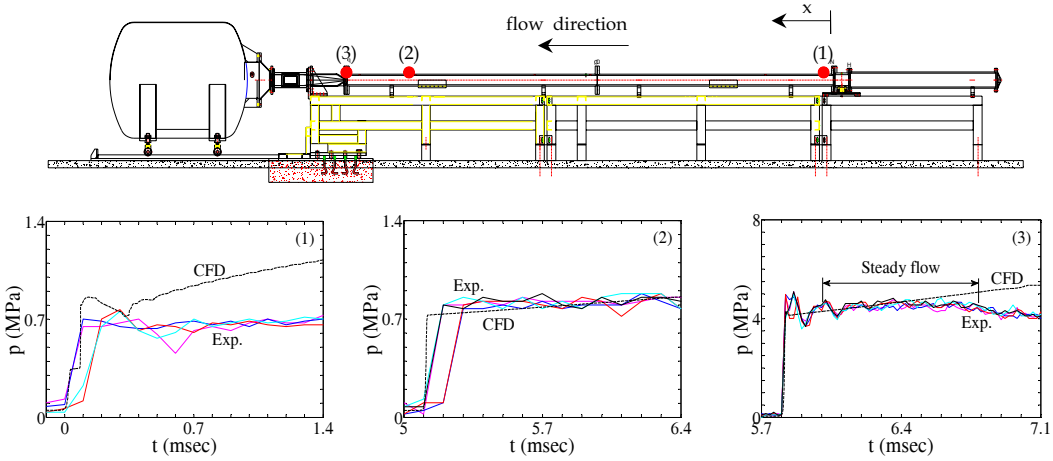

Fig. 5 Comparison of measured and calculated wall static pressures along the driven tube.

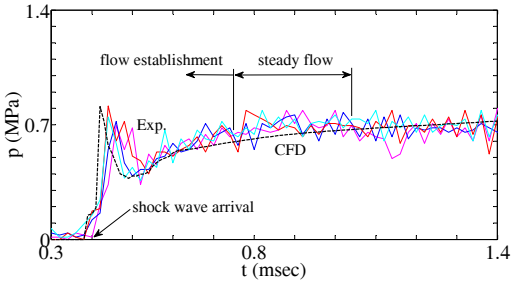

Fig. 6 Measured and calculated pitot pressures at the nozzle-exit center.

Table 2. Freestream flow condition.

Property	Value	Uncertainty(%)
p_∞ (kPa)	30.8	16
u_∞ (m/sec)	1610	1.8
$T_{\infty,tr}$ (K)	420	4.7
$T_{\infty,ve}$ (K)	1130	0.4
ρ_∞ (kg/m^3)	0.256	11
M_∞	4.02	4.2
Re_∞ (1/m)	16.5x10^6	17
h_o (MJ/kg)	1.47	3.1

traces are included to show the shot-to-shot repeatability.

The steep initial rise of the signal(at about 0.38 msec) is due to the shock wave arrival at the nozzle-exit. The flow then requires about 0.35 msec to establish in the nozzle. After the establishment period, the flow becomes steady. The flow remains steady for about 0.29 msec. During the steady flow, the measured pressure is 692(±2.6%) kPa.

The calculated pressure is 631(±8.0%) kPa which differs by 8.8% from the experiment.

Table 2 summarizes the calculated freestream flow condition at the nozzle-exit center during the steady flow. The thermodynamic properties were obtained by taking average values within a steady state. The flow was considered to be steady when the mean values for each signal trace reached 95% of their final values for pressure. The uncertainties(%) were calculated using the standard deviation of the properties based on the 2σ confidence interval.

In the table, the subscripts ∞ and o denote freestream and total conditions, respectively. The Reynolds number (Re) is based on ρu/μ where u is velocity and μ is viscosity. The symbol h denotes flow enthalpy. Other symbols have their usual meanings.

4.3 Scramjet

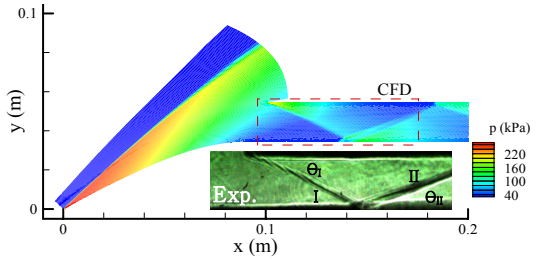

Fig. 7 A static pressure contour and a shock wave pattern in the combustor.

4.3.1 Without fuel injection and cavity

Fig. 7 shows the calculated static pressure contour around the scramjet model as well as the measured shock wave pattern inside the combustor during the steady flow. Flow direction is from left to right. Optical visualization images were obtained using a shadowgraph technique. The images were recorded using a high speed camera IDT XS4 with shutter speed of 0.4 μsec.

Looking at the optical image, the symbols I and II denote shock waves emanating from the cowl leading edge and a reflected shock wave of I, respectively. Θ_I and Θ_{II} denote associated angles of I and II bounded by the cowl and the scramjet body, respectively.

Regarding the CFD pressure contour, a clear-patterned shock train that is emanated from the cowl leading edge, is evident. At a slight distance upstream where the cowl shock reflects from the body surface, a small region of vortex-driven separated flow in the vicinity of the wall can be seen. A similar trend is also seen in the optical image. The vortex is likely to be formed due to the adverse pressure gradient downstream of the contoured-part of the wedge, which tends to interact with the incoming cowl shock. In front of the vortex, a separation shock wave is generated which tends to merge with the reflected cowl shock at sufficient distance downstream.

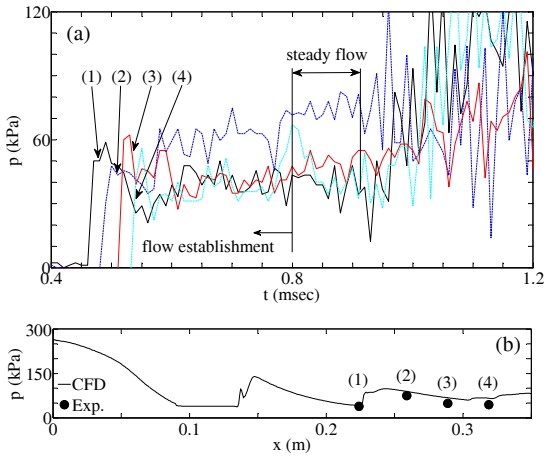

(a) Measured data; (b) Wall pressure distribution

Fig. 8 Wall pressures along the scramjet surface.

The measured Θ_I is found to be 26.5(±6.0%) deg. The calculated Θ_I is 25.6(±12.1%) deg, which differs by 3.4% from the experiment. Similarly, the measured Θ_{II} is 20.5(±12.5%) deg. The calculated Θ_{II} is 20.2(±14.0%) deg, which differs by 1.5% from the experiment.

Fig. 8 compares the measured wall static pressures along the scramjet surface with that of the calculated result. Fig. 8(a) shows the measured signal traces at different locations along the body which are designated as (1) to (4). The times are synchronized with respect to the shock wave arrival at the end-wall. Fig. 8(b) shows the calculated wall static pressure distribution along the scramjet surface. The measured values are also included for comparison.

Looking at Fig. 8(a), the flow requires about 0.42 msec(counting from the flow arrival at the leading edge) to reach a steady state in the combustor. The steady flow lasts for about 0.13 msec after which the measurement becomes unusable due to change in conditions which is believed to be due to the movement of separation point both in the nozzle and the

test section walls.

Regarding Fig. 8(b), the agreement between the measurement and the calculated results are fair in general but the calculated results show slightly higher pressures than that of the measured data especially in the downstream region. This discrepancy is likely to be inherited to the 3D nature of the flow in the combustor which is unable to be captured in the 2D simulation.

4.3.2 Ethylene injection data

Fig. 9 shows the optical images of the flow-field pattern in the combustor during the steady flow. The jet-to-freestream momentum flux ratio $J=(\rho u^2)_{inj}/(\rho u^2)_\infty$ used in the experiment was kept at about 3.1. The freestream condition herein denotes the combustor entrance condition. The images for the fuel injection was captured using a Schlieren technique. The images were recorded using a high speed camera Photron FASTCAM SA-X type 324K-C2 with shutter speed of 10 μ sec.

On the ramp of the cavity, it is evident that a series of compression waves coalescence to form a strong oblique shock wave, which may enhance the spreading rate of shear layer from the fuel injection and so enhanced mixing in supersonic flows.

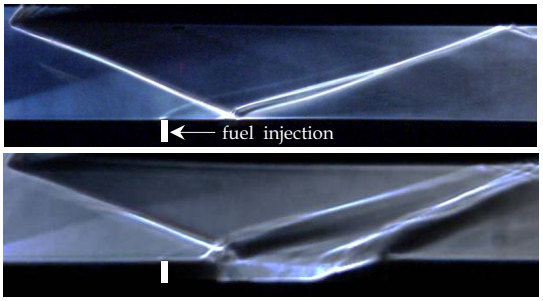

Fig. 9 Flow-field pattern in the combustor within steady flow.

Fig. 10 shows a chemiluminescence intensity signal captured by the Photron FASTCAM camera during the steady flow. In the figure, low enthalpy denotes the present condition. Whereas, high enthalpy denotes the off-design condition. The high enthalpy condition was generated by filling 4 MPa in the driver tube, 2 MPa in the transition section, and 0.013 MPa in the driven tube. This produced the flow to have total temperature of 2320(±1.0%) K. This is about 44 % higher than that of the present condition which is 1610(±2.3%) K. The off-design condition has steady flow duration of about 0.1 msec in the combustor judging from the measured wall static pressures along the scramjet surface.

Interestingly, the present condition shows a negligible level of chemiluminescence intensity indicating that there is no occurrence of combustion. On the other hand, the high enthalpy condition shows a strong level of chemiluminescence in the cavity as well as the region downstream. In our recent paper[21], auto-ignited flow-field and flame-holding characteristics of the ethylene jets have been experimentally examined using the shock tunnel. Flow visualization and CH^* chemiluminescence images were obtained using a broad range of conditions including the conditions presented in Fig. 10.

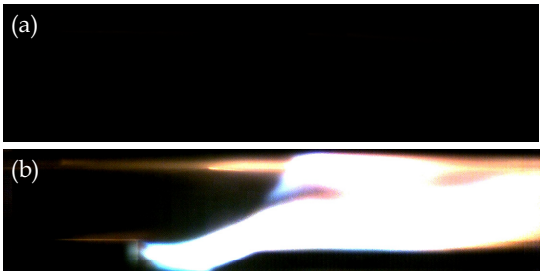

(a) low enthalpy; (b) high enthalpy

Fig. 10 Chemiluminescence intensity within steady flow.

The data showed that at 2080 K, the combustion was maintained inside the cavity and this condition provided a continuous ignition downstream of the cavity indicating that flame-holding is achieved. At 2320 K, a similar trend was found with that of the 2080 K condition. At temperatures lower than 2080 K, the flame-holding was not maintained.

In the region above the cavity in the vicinity of the cowl surface, although not strong but some level of pre-combustion looking signal is captured. This signal is generated due to vapourized hydrocarbon molecules flew from the driven tube wall that travel inside the hot boundary layer near the cowl surface which triggered the luminescence[21]. The high enthalpy condition corresponds to the freestream flow replicating a supersonic combustor environment for a Mach 7 flight speed.

5. Conclusions

In this work, the overall design, manufacture, and performance testing skills of the high speed propulsion system using the shock tunnel are presented. At the low flow enthalpy with total temperature of 1610 K, the ethylene auto-ignition did not occur. For the high enthalpy condition with total temperature of 2320 K, the strong level of chemiluminescence in the cavity as well as the region downstream was seen. One important contribution from the present work is that the occurrence of combustion using the short duration-based facility shock tunnel, which has not yet been confirmed by the Korean research community, has been verified. This opens the possibility for further scramjet testing using the shock tunnel in Korea.

References

1. Rowan, S.A. and Paull, A., "Performance of a Scramjet Combustor with Combined Normal and Tangential Fuel Injection," *Journal of Propulsion and Power*, Vol. 22, No. 6, pp. 1334-1338, 2006.
2. Stalker, R.J., Paull, A., Mee, D.J., Morgan, R.R. and Jacobs, P.A., "Scramjets and Shock Tunnels - The Queensland Experience," *Progress in Aerospace Sciences*, Vol. 41, pp. 471-453, 2005.
3. Hui, Y., Feng, L. and Baigang, S., "Trajectory Analysis of Fuel Injection into Supersonic Cross Flow Based on Schlieren Method," *Chinese Journal of Aeronautics*, Vol. 25, Issue 1, pp. 42-50, 2012.
4. Razzaqi, S.A. and Smart, M.K., "Hypervelocity Experiments on Oxygen Enrichment in a Hydrogen-Fueled Scramjet," *AIAA Journal*, Vol. 49, No. 7, pp. 1488-1497, 2011.
5. Kang, S.H., Lee, Y.J. Yang, S.S., Smart, M.K. and Suraweera, M.V., "Cowl and Cavity Effects on Mixing and Combustion in Scramjet Engines," *Journal of Propulsion and Power*, Vol. 27, No. 6, pp. 1169-1177, 2011.
6. Osgerby, I.T., Smithson, H.K. and Wagner, D.A., "Supersonic Combustion Tests with a Double-Oblique-Shock Scramjet in a Shock Tunnel," *AIAA Journal*, Vol. 8, No. 9, pp. 1703-1705, 1970.
7. McIntyre, T.J., Houwing, A.F.P., Palma, R.C., Rabbath, P.A.B. and Fox, J.S., "Optical and Pressure Measurements in Shock Tunnel Testing of a Model Scramjet Combustor," *Journal of Propulsion and Power*, Vol. 13, No. 3, pp. 388-394, 1997.
8. Wendt, M.N. and Stalker, R.J., "Transverse and Parallel Injection of Hydrogen with

Supersonic Combustion in a Shock Tunnel," *Shock Waves*, Vol. 6, Issue 1, pp. 53-59, 1996.

9. Stalker, R.J., Morgan, R.G. and Paull, A., "A Shock Tunnel Investigation of Scramjet Performance with Partially Premixed Combustion," *7th AIAA International Space Planes and Hypersonic Systems and Technologies Conference,* Norfolk, VA., U.S.A., AIAA-96-4534, Nov. 1996.
10. Ben-Yakar, A., Mungal, M.G. and Hanson, R.K., "Time Evolution and Mixing Characteristics of Hydrogen and Ethylene Transverse Jets in Supersonic Crossflows," *Physics of Fluids*, Vol. 18, No. 2, 026101, 2006.
11. Ben-Yakar, A. and Hanson, R.K., "Ultra-Fast-Framing Schlieren System for Studies of the Time Evolution of Jets in Supersonic Crossflows," *Experiments in Fluids*, Vol. 32, pp. 652-666, 2002.
12. Yang, I., "Design and Performance Evaluation of a Liquid-Fueled Scramjet Engine Model," PhD Dissertation, KAIST, Daejeon, Korea, 2013.
13. Jacobs, P.A., "Shock Tube Modelling with L1d," Report 13/98, Department of Mechanical Engineering, The University of Queensland, Brisbane, Australia, 1998.
14. Gollan, R.J., "Yet Another Finite-Rate Chemistry Module for Compressible Flow Codes," Report 9/2003, Department of Mechanical Engineering, The University of Queensland, Brisbane, Australia, 2003.
15. Mallinson, S.G., Mudford, N.R. and Gai, S.L., "Pitot Pressure Survey of the 1/2" Throat 12" Exit Conical Nozzle for the T3 Free-Piston Shock Tunnel," Aerospace Technical Report 92-1, University of New South Wales, Australian Defence Academy, Canberra, Australia, 1992.
16. Brieschenk, S., O'Byrne, S. and Kleine, H., "Laser-Induced Plasma Ignition Experiments in a Scramjet Inlet," *49th AIAA Aerospace Sciences Meeting including the New Horizons Forum and Aerospace Exposition,* Orlando, FL., U.S.A., AIAA-2011-504, Jan. 2011.
17. Park, G., "Hypervelocity Aerothermodynamics of Blunt Bodies Including Real Gas Effects," PhD Dissertation, The University of New South Wales, Canberra, Australia, 2010.
18. Jacobs, P.A., "Eilmer's Theory Book: Basic Models for Gas Dynamics and Thermochemistry," Report 2010-09, The University of Queensland, Brisbane, Australia, 2010.
19. Park, C., "Nonequilibrium Hypersonic Aero thermodynamics," John Willey & Sons, New York, N.Y., U.S.A., 1990.
20. Park, G., Choi, H., Byun, J., Jin, Y. and Hwang, K., "Characteristic Study of Fuel Injection into a Supersonic Flow in a Shock Tunnel," *40th KSPE Spring Conference*, pp. 290-297, 2013.
21. Park, G., Park, C., Jin, Y., Choi, H., Byun, J. and Hwang, K., "Ethylene Transverse Jets in Supersonic Crossflows," *Journal of Propulsion and Power*, In press.